Acquisition footprint suppression on 3D land surveys

Necati Gulunay,[1] Nigel Benjamin,[2] and Mag Magesan[1] of CGG discuss the acquisition geometry footprint that occurs on most 3D land surveys and a robust method to attenuate it.

Acquisition geometry footprint on 3D land surveys manifests itself as striping on time slices of stack volumes with inline and crossline periods that coincide with the source and receiver line intervals of the acquisition geometry. Hill et al. (1999) give a detailed description and analysis of acquisition footprint. DMO volumes are also known to exhibit such artefacts. Schleicher et al. (1989) and Ronen (1994) address DMO artefacts caused by irregularities in the fold pattern.

These artefacts on stack volumes (or DMO volumes) are sometimes described as 'hatching' or 'chatter' and they hinder accurate interpretation. This phenomenon is similar to the periodic artefacts that are observed along the inline (CDP) direction of 2D lines where patterns are due to the fact that the offset distribution within CDPs shows a periodicity proportional to the ratio of the source interval divided by the receiver interval. In 2D surveys, shot and receiver geometry and field arrays can be combined via the 'stack array' principle (Ansty, 1986; Morse et al., 1989) to attenuate such artefacts.

It is well known that such artefacts in 2D can be reduced by alias handling trace interpolation as the source of the problem is the steeply dipping (aliased) energy formed from use of sparse recording geometries. In 3D land surveys, owing to large source and receiver line intervals, and due to the quest for small source and receiver arrays, it is not possible to apply the 'stack array' principle. Any multichannel process, whether it is stack, DMO, or migration, is prone to such artefacts. As interpolation is difficult or costly other means to attenuate such artefacts are required.

The first published observations known to us of acquisition footprint problems on 3D volumes and a deterministic solution for their attenuation were made by Meunier et al. (1992) and Baixas et al. (1993). Shortly afterwards Gulunay et al. (1994) suggested a data-adaptive frequency-wavenumber domain notch filtering method that worked well for data with generally flat events. Gulunay (1999, 2000) later extended the method to dipping data by observing that the artefact shapes are frequency-invariant but that their location varies with frequency and follows the dip of each dominant event.

Working in the frequency domain is not the only tool: Drummond et al. (2000) suggested the use of time slices and wavenumber domain deterministic notch filtering on those slices. However, because their time slice based filtering method was not data-adaptive and noise patterns can vary with time, they also suggested the use of adaptive subtraction of the noise. Geometry-driven deterministic time slice filtering of 3D data for footprint attenuation was later proposed by Soubaras (2002). Karagul et al. (2004) showed interesting results on a data set with complex structures using the Soubaras approach. Most recently, Al-Bannagi et al. (2004) proposed time slice singular value decomposition (SVD) filtering where footprint attenuation and random noise attenuation are performed in one step by selecting certain singular values.

Seeing such prior publications one might naturally wonder what the pros and cons of working in time or frequency slices are, as they are not necessarily the same even when all the frequencies are filtered in the frequency domain method. One might also wonder if data-adaptive methods like the ones by Gulunay (1999, 2000) can handle complex field patterns or whether we should design deterministic filters for each separate study. Leaving the first question to future studies, Gulunay et al. (2005) have developed a frequency slice wavenumber notch filtering method, named FKF3D, with extensive user controls and some important QC capabilities, and have tested it on various data sets from the Middle East. In this paper we give an introduction to the underlying principles of the method and show some results on Middle East field data.

Spatially periodic noise forms spikes in the wavenumber domain

A simple model can be used to illustrate the principles of the FKF3D method. A repetitive noise train shows itself in the wavenumber domain as spikes superimposed on the signal spectrum. This noise can be attenuated by simply scaling the spikes in this domain. For the model let us form a 50-point signal, $\mathbf{s}$, with a decay from value 10 to value 5 (depicted by the red curve in Figure 1). Let us also form a 50-sample noise model, $\mathbf{n}$, using a five sample (-2,-

[1] CGG Americas Inc, Houston, Texas.
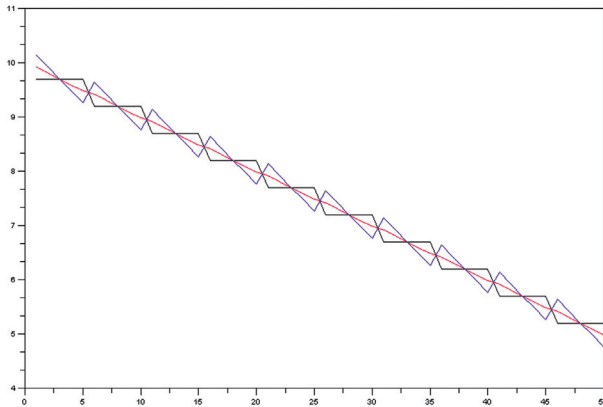[2] CGG Dedicated Centre for PDO, Muscat, Oman.

1,0,+1,+2) wavelet that is repeated 10 times (depicted by the blue curve in Figure 1).

Note that such a repetition can be considered as a convolution of this short noise wavelet with a comb function in space

$$\text{comb}_5(x) = (1,0,0,0,0,1,0,0,0,0,1,0,\dots)$$

where the subscript shows the wavelength. There are 10 spikes in this comb function (as hinted by the blue curve in Figure 1). The sum, **d=s+n**, of signal and noise is depicted by the green curve in Figure 1.

The wavenumber spectrum of the signal, **S**, is shown in Figure 2. As seen, owing to spatial variation in the signal, there are non zero signal components at all wavenumbers.

The wavenumber spectrum of the noise, **N**, is shown in Figure 3. Note that a Fourier transform (FT) of the above comb function of x (in space) is another comb function in wavenumber (k).

$$\text{FT}(\text{comb}_N(x)) = \text{comb}_{1/N}(k)$$

where subscripts N and 1/N show the periodicity for x and k respectively.

In this example, because the periodicity is 1/5 in the wavenumber domain, there will be five spikes in this domain. However, although we observe that the noise spectrum in Figure 3 comprises spikes, we also observe that the magnitude of these spikes is not constant and that one spike is missing. These observations are because convolution is a product in the wavenumber domain. The noise spectrum **N** can be interpreted as the sampled version of the broad spectrum formed by a short noise wavelet (-2,-1,0,1,2) with this comb function. The reason that the 5th spike (that should be at k=0) is missing is because the repetitious wavelet in space has no DC component.

The wavenumber spectrum of signal plus noise is shown in Figure 4. Note that this figure closely resembles spectra that occur in the wavenumber domain for real data.

Figure 1 *An example of jittery one-dimensional data (green) made of smooth signal (red) and repetitive noise (blue).*

Figure 3 *Wavenumber spectrum of the noise (blue) from Figure 1.*

Figure 2 *Wavenumber spectrum of the signal (red) from Figure 1.*

Figure 4 *Wavenumber spectrum of the data (signal plus noise - green) from Figure 1.*

Figure 5 *Reconstructed signal with scale factor a=0.2 (blue), a=0.1 (red) and a=0.0 (black).*
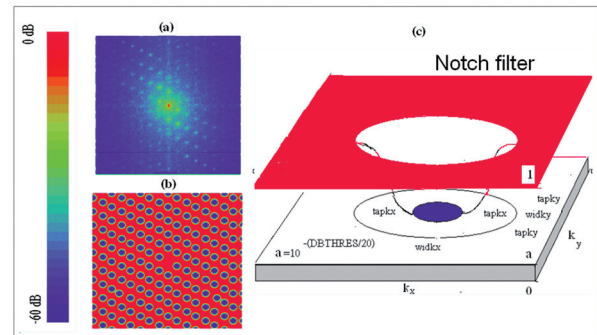

Figure 6 *a) An example of an average k_x-k_y spectrum, b) the predetermined notch filters in k_x-k_y domain, and c) the shape of the notch filter in k_x-k_y domain.*

Comparing this with the signal spectra in Figure 2, we see that the effect of adding noise to signal is to add these four spikes to data in the wavenumber domain (k=-0.4, k=-0.2 , k=+0.2, and k=+0.4). By scaling the value of the total spectrum at these points with constant scale factors of 0.2, 0.1, and 0.0, and inverse transforming back to space, we obtain the blue, red, and black curves depicted in Figure 5. Scale factor 0 is too small and scale factor 0.2 is too large, whilst scale factor 0.1 is about right. This simple example suggests that by scaling down the values of the spikes with proper values, in this case a factor of 0.1, the signal components will be reliably retrieved.

The above analysis is given in only one space dimension for simplicity. It can easily be extended to two space dimensions. When data are flat they show the same footprint pattern at all frequencies, and these patterns are centred at zero wavenumber. By summing data responses across frequencies one can obtain a reliable form of the footprint for easy detection of points that need scaling down (Gulunay 1994). When data have significant dip then artefacts appear centred at each dipping event and one needs to follow dipping events in the f-k or f-k_x-k_y domain (Gulunay 1999, 2000).

FKF3D method
We use similar considerations given above in our method called FKF3D, and process 3D volumes in small time-space(x)-space(y) cubes. The typical size of this cube is 400 ms x 100 inlines x 100 crosslines. These cubes overlap by 50% in all dimensions to form the final 3D volume. For each cube we can form four diagnostic plots a) input kx-ky spectrum, b) local maxima detected, c) final filter, and d) output kx-ky spectrum.

Figure 6a shows an average k_x-k_y spectrum obtained from one set of field data in a shallow cube as described above. The centre of the k_x-k_y spectrum is where the data resides and the greenish yellow spots around it are the spikes that need to be attenuated. Location of these spikes can be detected automatically. Additionally the amplitude of these spikes is observed to

decay as one travels away from the centre. If these patterns are stationary then one can impose a pattern as seen in Figure 6b. The shape of the filter that we use for 3D data at each spike location found is shown in Figure 6c. It is a scaling function that is equal to one outside an outer ellipse (red zone) and equal to a constant scalar less than one inside an inner ellipse (blue zone). A radial cosine taper takes place in-between. As data are processed in temporal windows then the value of the attenuation level can be made time varying. Stronger footprint patterns show at shallow record times (e.g. in mute zones) and here more attenuation of these spikes may be desirable. The sizes of the inner and outer ellipses also control the effectiveness of the filter.

Having space windows and automatic detection of spike locations also facilitate processing of merged surveys. Note that the centre of the k_x, k_y response (as they are always aligned at the event) is occupied by signal and must be protected during the process.

Field data examples
We have experimented using stacked data resulting from a number of different 3D geometries amongst which are those more commonly referred to as 'Single Zig-Zag', 'Double Zig-Zag' 'Triple Zig-Zag', 'Shifted Double Zig-Zag' and 'Checker-Board'. Each of these represents a sparse 3D acquisition with variations in source and receiver density and surface location layout. As a consequence, they each have a different acquisition footprint. Here we will present the results from three of these experiments. Figure 7 shows source and receiver configurations for a layout known as Double Zig-Zag geometry. Figure 8a shows the k_x-k_y spectrum generated by FKF3D (in the time window 0-400 ms of the first space window of size 100 lines and 100 crosslines). This plot represents the accumulated k_x-k_y spectrum found from data on all frequency slices in that time window. The red colour is the peak (0 dB value), yellow is about -30 dB, and blue is about -60 dB. Spatial periodicity that exists in the surface layout translates to spectral peaks in the k_x-k_y domain in this fashion (x=crossline, y=line).

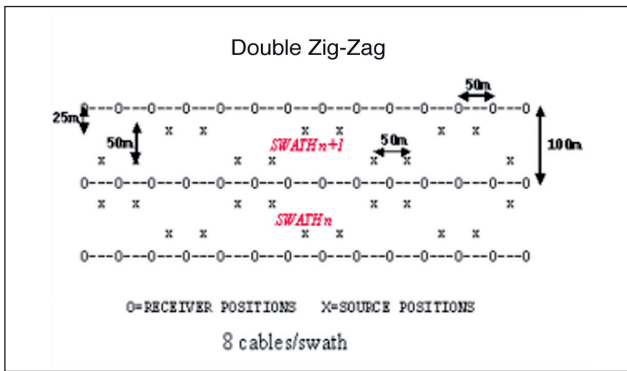**Figure 7** *Double Zig-Zag field configuration (x=shot, o=receiver).*
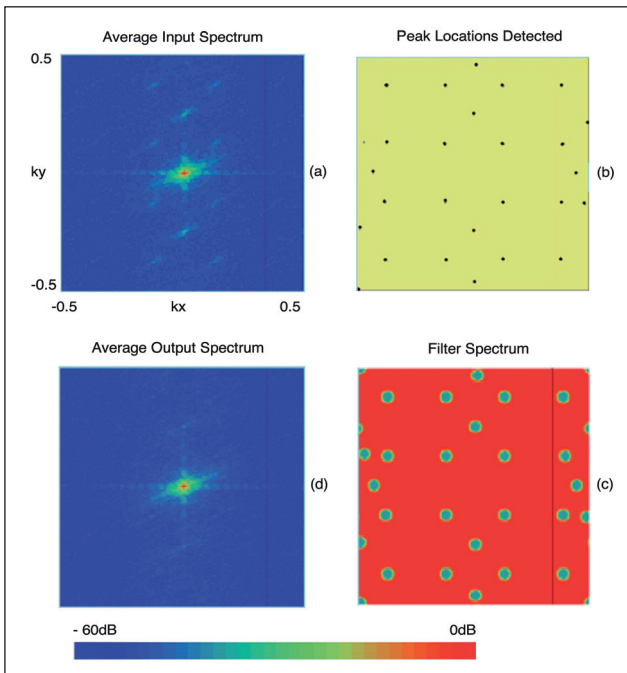

Figure 8 *Double Zig-Zag data FKF3D QC plots - a) k_x-k_y spectrum estimated by FKF3D for a shallow time-space window, b) local maxima, c)- filter, and d) output*
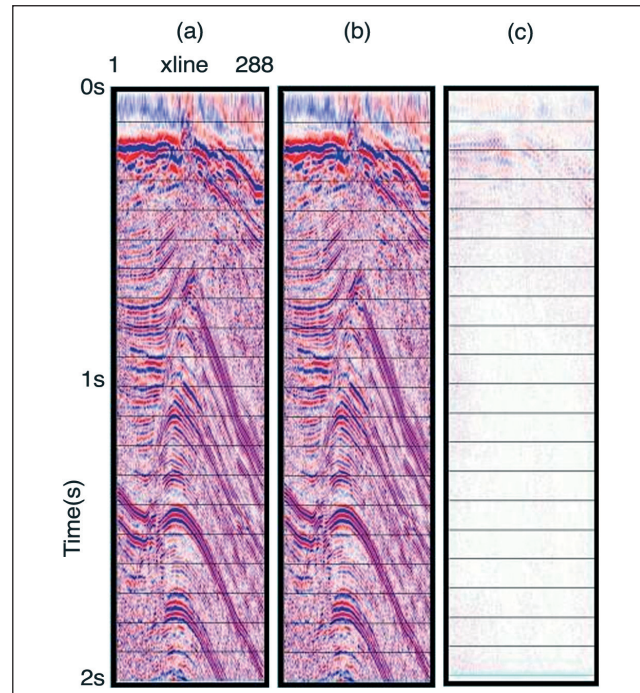

Figure 9 *An inline from data with double Zig-Zag geometry - a) input, b) output, and c) difference.*
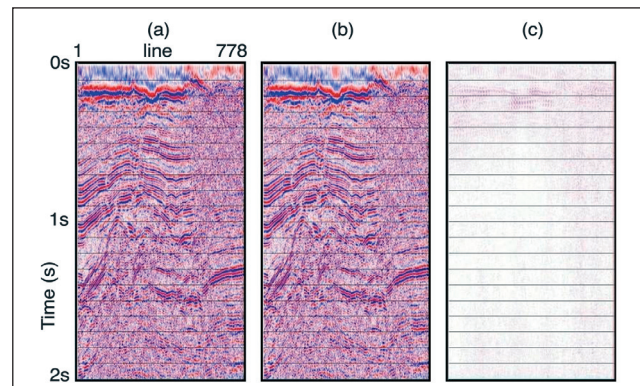

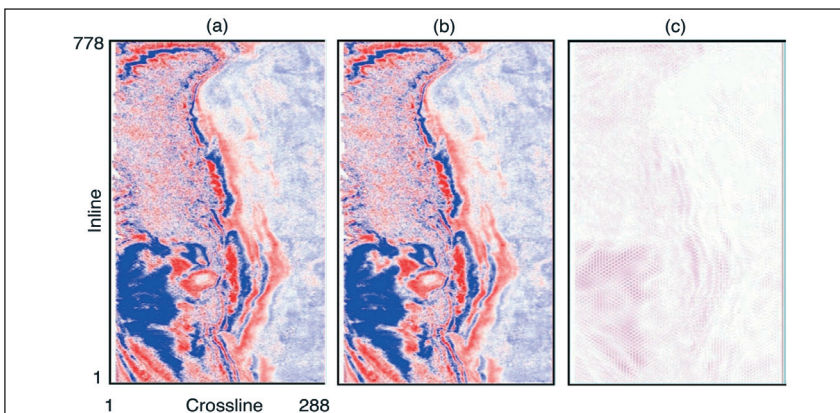**Figure 10** *A crossline from data with Double Zig-Zag geometry - a) input, b) output, and c) difference.*

Figure 11 *A time slice (200 ms) from data with Double Zig-Zag geometry - a) input, b) output, and c) difference.*

Figure 8b shows the local maxima detected by FKF3D. Figure 8c is the filter to be applied to data in that time window. Note that red is 0 dB and grey is -36dB. Figure 8d shows the average k_x-k_y spectra after the filter has been applied to data on the frequency slices. The peaks are suppressed well while the data point (k_x=k_y=0) is well preserved

Figures 9a, b, and c show input, output, and difference sections respectively, on one of the inlines of this survey. Note the complex time structures on this data. Figures 10a, b, and c show the corresponding sections from a crossline. It is clear that FKF3D preserved the structured data whilst suppressing the footprint that existed in the shallow time windows. Figures 11a, b, and c show the time slices of input, output, and the difference respectively, at 200 ms. The footprint shows clearly on the difference section (Figure 11c).

Figure 12 shows another survey geometry from the Middle East known as Shifted Double Zig-Zag. In Figure 13a we see spatial periodicity clearly forming as spectral peaks in the k_x-k_y domain of the shallow (0-400 ms) time-space window. Figures 13b, 13c, and 13d show respectively, the local maxima detected by FKF3D, the final filter, and the k_x-k_y spectra after application of the filter to this time-space window. On Figures 14a, b, and c, we see the input, output and difference sections respectively, for a time slice at 400 ms. Corresponding sections of a line and crossline are given in Figures 15 and 16.

Figure 17 shows another survey geometry from the Middle East known as Shifted Triple Zig-Zag and the k_x-k_y spectrum obtained from data in a shallow time window. Again, we see spatial periodicity clearly forming as spectral peaks in the k_x-k_y domain of the shallow (0-400 ms) time-space window. Figure 18 shows the results of the process on a crossline for the first second of data. Figures 19a, b, and c show input, output, and, difference time slices, respectively, at 200 ms.
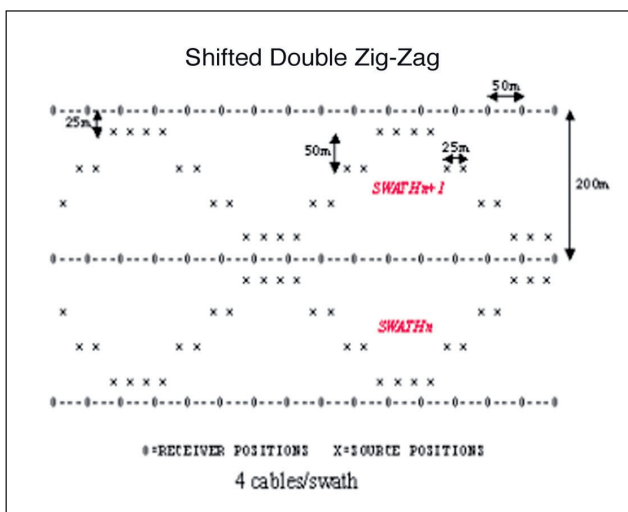
Discussion

One might wonder if the method discussed can handle any spatial periodicity. We showed above that a spatial periodicity of N traces give N spikes in the wavenumber domain. In two space dimensions, N_x length periodicity along the x direction and N_y length periodicity in the y direction produces N_x*N_y peaks in the wavenumber domain. As N_x and N_y get larger and larger more and more peaks are produced in the k_x-k_y plane. The separation between these peaks consequently gets smaller and smaller. This means that not only will too many points be touched by the filter but also that protection of the origin will become more difficult as there will be peaks very close to the origin that ought to be suppressed. With typical small space gates (100 inlines, 100 crosslines) used in the method (due to structural complexity) we find that there is not enough resolution to precisely filter out such artefacts.

Conclusion

We observed in this study that 3D acquisition footprints can be effectively attenuated on many different acquisition geometries on data with moderate to complex geology without causing harm to underlying data using wavenumber domain notch filters on frequency slices.
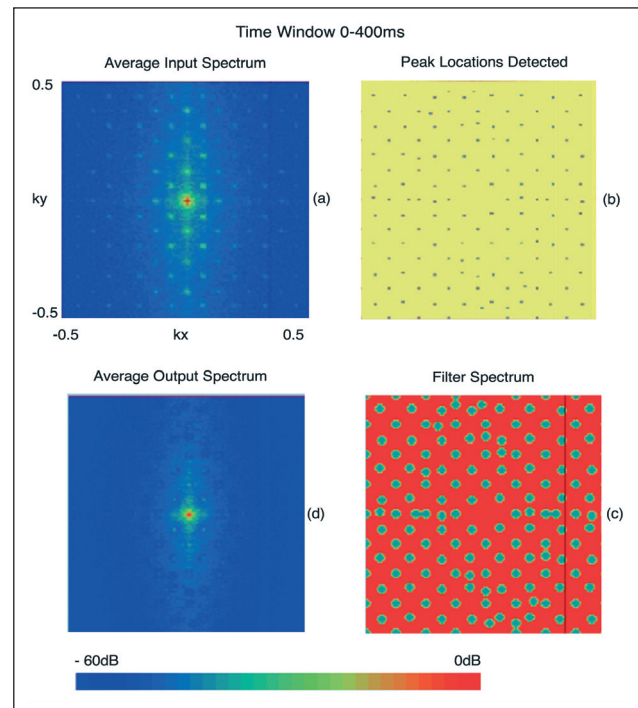
Acknowledgments

Figure 13 *Shifted Double Zig-Zag data FKF3D QC plots - a) k_x-k_y spectrum estimated by FKF3D for a shallow time-space window, b) local maxima, c) filter, and d) output.*
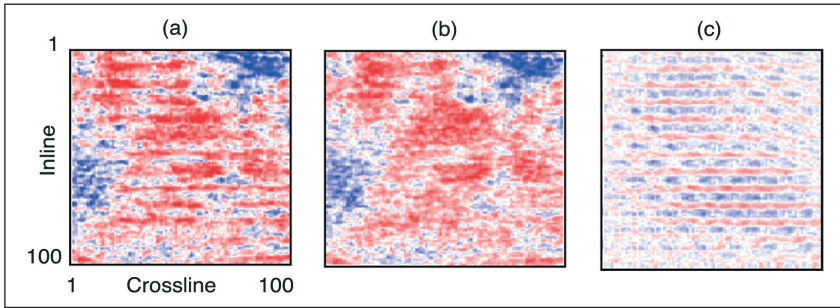

Figure 12 *Shifted Double Zig-Zag field configuration (x=shot, o=receiver).*

Figure 14 *A time slice (400 ms) from data with Shifted Double Zig-Zag geometry - a) input, b) output, and c) difference.*
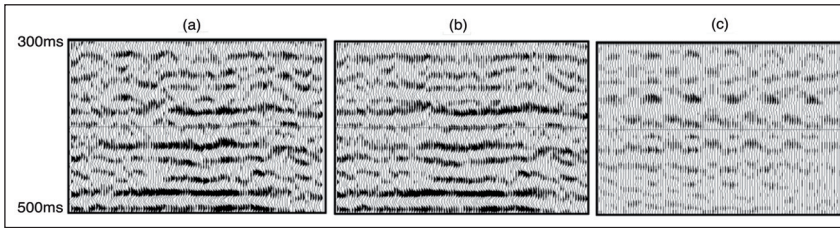

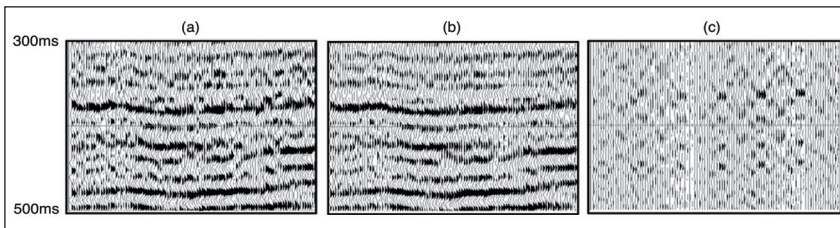**Figure 15** *An inline from data with Shifted Double Zig-Zag geometry - a) input, b) output, and c) difference.*

Figure 16 *A crossline from data with Shifted Double Zig-Zag geometry - a) input, b) output, and c) difference.*
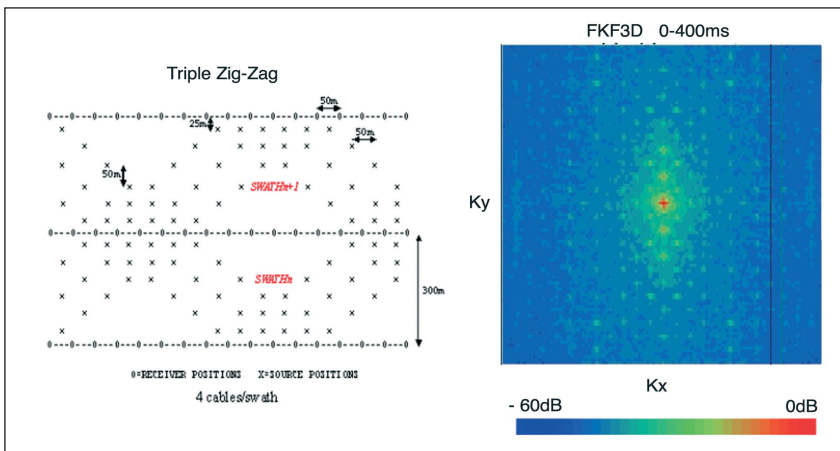

Figure 17 *Shifted Triple Zig-Zag field configuration (x=shot, o=receiver) and k_x-k_y spectrum estimated by FKF3D for a shallow time-space window.*

References

Al-Bannagi, M.S., Fang, K., Kelamis, P G., and Douglass, G. S. [2004] Acquisition footprint suppression via the truncated SVD technique. *74th SEG Annual International Meeting.*

Ansty, N. A. [1986] Whatever happened to ground roll? *Leading Edge*, **5**, 40-45.

Baixas, F. and, Meunier, J. [1993] Examples of methods for counteracting artefacts and errors in 3D seismic surveys. *SEG Summer research workshop*, Expanded Abstracts.

Drummond, J., Budd, B. and Ryan, J. [2000] Adapting to noisy 3D data - attenuating the acquisition footprint. *70th SEG Annual International Meeting*, 9-12.

Gulunay, N., Martin, F., and Martinez, R. [1994] 3D data acquisition artefacts removal - spot editing in the spatial-temporal frequency domain. *56th EAGE Annual Conference*, Session: H049.
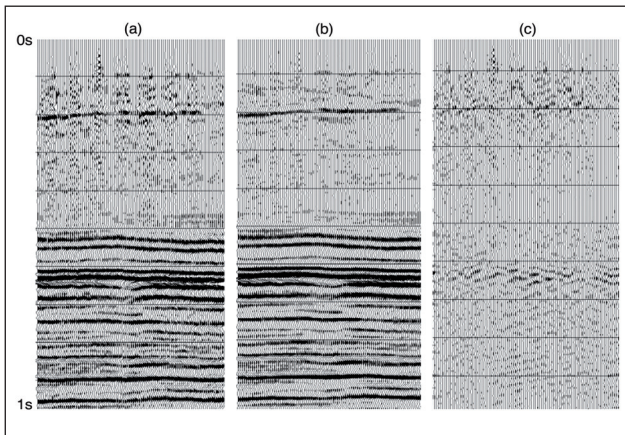
Figure 18 *A crossline from data with Shifted Triple Zig-Zag geometry - a) input, b) output, and c) difference.*
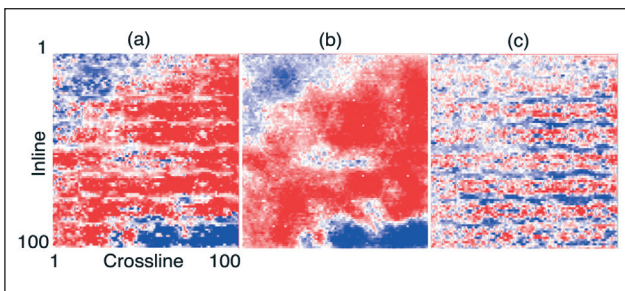

Figure 19 *A time slice from data with Shifted Triple Zig-Zag geometry – a) input, b) output, and c) difference.*

Gulunay, N. [1999] Acquisition geometry footprints removal. *69th SEG Annual International Meeting*

Gulunay, N. [2000] 3D acquisition footprint removal. *62nd EAGE Annual Conference*, Session: L0017.

Gulunay, N., Benjamin, N., and Magesan, M. [2005] Footprint suppression with wavenumber notch filtering for various acquisition geometries, *67th EAGE Annual Conference*

Hill, S., Schultz, M. and Brewer, J. 1999] Acquisition footprint and fold-of-stack plots. *The Leading Edge*, **18**, 6, 686-695.

Karagul, A., Crawford, R., Sinden, J., and Ali, S. [2004] Recent advances in 3D land processing: Examples from Pakistan Badin Area. *First Break*, **22**, 9, 37-40.

Meunier J. and Belissent, M. [1992] Reduction of 3D geometry generated artifacts. *6th Venzualean Congress*.

Morse, P. F. and Hildebrandt, G. F. [1989] Ground-roll suppression by the stackarray. *Geophysics*, **54**, 3, 290-301.

Ronen, S. [1994] Handling irregular geometry: Equalized DMO and beyond. *64th SEG Annual International Meeting*, 1545-1548.

Schleicher, K. L. , and , Black, J. L. [1989] Effect of irregular sampling on prestack DMO. *59th SEG Annual International Meeting*, 1144-1147.

Soubaras, R. [2002] Attenuation of acquisition footprint for non-orthogonal 3D geometries. *64th EAGE Annual Conference*.